World Conference on Timber Engineering Oslo 2023

EXPERIMENTAL AND NUMERICAL INVESTIGATION ON THE EFFECT OF CIRCULAR HOLES ON GLULAM COMPOSITE BEAMS

Dag Pasquale Pasca[1], Yuri De Santis[2], Angelo Aloisio[3], Andreas Stenstad[4], Karl-Christian Mahnert[5],

ABSTRACT: This paper presents an extensive experimental investigation on the effect of circular holes with and without reinforcement on glulam joists' behaviour. The tests consider the variability of hole position, number and strength class of the beam. Furthermore, a finite element model based on fracture mechanics was developed and validated against the experimental force-displacement curves of thirteen configurations. The model reproduces crack initiation and propagation through the adoption of cohesive contact layers. The satisfactory agreement with the experimental data has been the base of extensive parametric analyses considering multiple beam and hole geometry selections and two load arrangements at the upper and lower side of the beam. Finally, the results of the parametric analyses, initially used for a qualitative understanding of the structural behaviour, are used for calibrating probabilistic capacity models of the capacity of simply-supported beams with circular holes. The mechanics-based probabilistic model calculates the capacity as the product between the analytical capacity associated with the reduced cross-section and an adimensional correction factor. The factor is expressed as a linear combination of a set of explanatory variables selected after a step-wise deletion process.

KEYWORDS: Holes; Glulam; Reinforcement; NLFM; Experimental tests; FEM.

1 INTRODUCTION

The use of holes in timber beams is a widespread structural solution, especially in the case of interference with pipeline services. The occurrence of tensile stresses perpendicular to grain due to holes, shrinkage, external loads, or a combination of these factors in timber beams can significantly impair the bearing capacity, given the low tensile strength perpendicular to grain [1-3].
Most existing research on beams with holes focuses on experimental tests rather than numerical modelling [4-6]. Experimental tests [7], finite element analysis [8, 9], analytical modelling and design provisions [10] demonstrated the detrimental impact of the holes and notches on the load carrying capacity of the bare timber beams (without slabs) as well as timber composite I-joist with oriented strand board (OSB) webs [11].

The failure of timber beams with openings is typically associated with cracks initiated from the top quarter of the holes (towards mid-span) and/or from the bottom quarter of the holes (towards the support). Similar failure modes and delamination and shear failure of the flanges have been observed in the timber I-joists with web openings [11-13]. The results of laboratory testing and FE modelling have been used to develop empirical equations for estimating the load-carrying capacity of the timber I-joists with web openings [14, 15]. Moreover, for the practical design of OSB webbed timber I-joists with openings, critical (minimum) spacing between the web openings was determined based on the results of FE analyses [15]. To minimize the impact of openings and notches on the peak load of the timber beams, different methods such as externally bonded plywood/OSB and steel plates [12, 13], and fully threaded screws or glued-in rods have been proposed. Their performance has been experimentally and analytically examined by [16, 17].

Karimi and Valipour [18] tested eleven different types of Laminated Veneer Lumber- Cross Laminated Timber (LVL-CLT) and Glued Laminated Timber (GLT)-CLT beams and four types of bare LVL-GLT beams without and with circular and square openings in the LVL-GLT webs under three-point bending to produce benchmark experimental data required for assessing the effect of the web openings on the failure mode and load carrying capacity of the Timber-Timber-Composite (TTC) beams. In addition, digital image correlation (DIC) was used to capture the strain profile around the holes up to the initiation of cracks (onset of fracture) and shed light on failure mechanisms generated by the combination of bending, shear, and tension perpendicular to the grain.

[1] Dag Pasquale Pasca, Norsk Treteknisk Institutt (Norwegian Institute of Wood Technology), Norway, dpa@treteknisk.no
[2] Yuri De Santis, Department of Civil Engineering, University of L'Aquila, Italy
[3] Angelo Aloisio, Department of Civil Engineering, University of L'Aquila, Italy
[4] Andreas Stenstad, Norsk Treteknisk Institutt (Norwegian Institute of Wood Technology), Norway
[5] Karl-Christian Mahnert, Norsk Treteknisk Institutt (Norwegian Institute of Wood Technology), Norway

https://doi.org/10.52202/069179-0353

Several capacity models underestimate the peak loading capacity of timber beams or maybe only applicable to the beams with specific details or cross-section dimensions. For instance, Danielsson [3] showed that the empirical method adopted in the Swedish glulam handbook [10] tends to underestimate the experimental load-bearing capacities of the GLT beams with rectangular openings.
Karimi and Valipour [19] numerically investigate the structural behaviour of the LVL and GLT beams with openings and highlight the importance and need for applying robust localization limiters (regularisation technique).
Recently, Gilbert et al [20] carried out tests on timber Circular Hollow Section (CHS) beams showing failure modes not usually encountered in timber structures.

Fracture mechanics approaches are needed for accurate predictions of the post-elastic behaviour of beams with holes [21]. Therefore, complex mechanical formulations are required, like those based on linear elastic fracture mechanics (LEFM) [22-24] and Weibull theory-based damage model [25].
Nonetheless, the predictions with LEFM might lead to conservative results, as highlighted by Adalany et al. [26], who considered LVL beams with holes.

Guan and Zhu [27] developed a nonlinear finite element model capable of simulating crack propagation based on stress monitoring. The model eliminates the structural contribution by setting the stiffness to zero when the yield strength is reached. However, despite the mentioned improvement, the model does not allow sudden crack propagation, typical of the shear failure of beams with holes.

More recently, methods based on nonlinear fracture mechanics (NLFM) proved to be more effective and capable of simulating the post-failure behaviour with crack propagation [21, 28].
Ardalany et al. [21] developed an NLFM-based tridimensional FE model to investigate the effect of shape, size and position of the openings of a glulam beam and to derive an optimal reinforcement strategy. Continuum damage models (CDM) were developed by Sandhaas [29] and modified by Gharib et al. [30] who enriched it with an anisotropic non-local integral-type model. The non-local CDM is implemented in FE software and then is employed to predict the nonlinear behaviour and capture failure of timber under complex multiaxial stress states generated by the presence of holes/openings.

This paper presents an experimental and numerical study on composite glulam joists with one or two circular holes in different positions. The experimental campaign aims at identifying the influence of hole position, hole number and distance on the reduction of the joist capacity. Furthermore, a finite element model, which accounts for crack initiation and propagation, is developed and validated against the experimental results. Differently from what has been done by [21], cohesive contacts have been used to reproduce the crack formation. The efficient tridimensional FE model has been parameterized and used to extend the results of the experimental campaign.

In synthesis, the main aspects of novelty and originality of this research are:

- Extensive experimental campaign on glulam joist with different hole geometry, position and reinforcement.
- Validation of a nonlinear finite element model based on fracture mechanics.
- Parametrization of the model and extensive analyses to assess the dependence of the capacity of beams with circular holes by varying the following parameters: hole diameter and position, beam geometry, the position of the load (upper side and lower side).

The main limitations of this research are twofold. The first relates to the experimental tests, where only one value for the hole-depth ratio was considered. Therefore, the FE model has only been validated for a specific hole/depth ratio. The second aspect relates to the computational burden of the analyses. The authors only varied the geometric parameters of the beam, assuming deterministic mechanical parameters, which were validated against the experimental tests. Future research efforts will assess the effect of the fracture mechanics properties by considering suitable probability distributions, thus providing a probabilistic estimate of the capacity for given geometric configurations.

2 EXPERIMENTAL TESTS

2.1 MATERIALS AND CONFIGURATIONS

The experimental campaign involved glue-laminated timber joist of length l=5700 mm, with a cross-section width b of 36 mm or 48 mm and with a cross-section height h of 300 mm (Figure 1).
In addition to the reference configurations without holes, joists with one or two holes of diameter d=170 mm in different positions along the joist axis were tested. The tests include configurations with a hole at mid-span and configurations with one or two holes near the supports or under the loading point. The position of the holes of each configuration is shown in Table 1.

Two different series have been considered to assess the glulam class influence on the mechanical properties reduction due to holes. The joists of both series are combined glulam with 19 mm thick ungraded internal lamellae and 47 mm thick external lamellae. The external lamellae of the first and second series are made of C30 and C40 lamellae, respectively. The mean density of the specimens is 460 kg/m^3
The tests covered both unreinforced beams and beam reinforced by glulam or plywood plates glued to the outer faces of the beams. Figure 2 shows the geometry and dimensions of the specimens with exterior reinforcements of the holes.

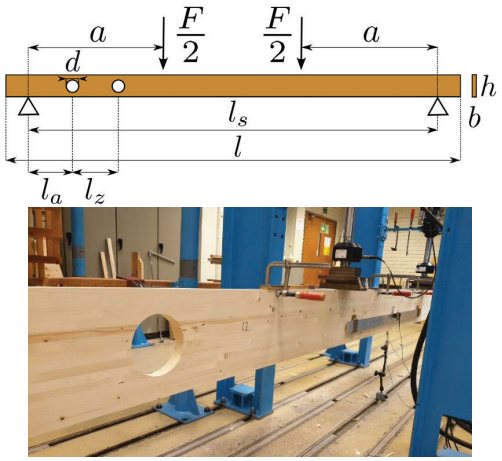

Figure 1 - *(up) Geometric configuration of the beam; (down) Experimental setup*

The plywood plate reinforcement has a length b_r of 1200 mm, a height h_r of 290 mm and a thickness t_r of 12 mm. The employed plywood has 5 layers and belongs to strength class F20/15 and MOE class E 45/25 according to EN 13986 and EN 636. The glulam reinforcement is made of the same material as the reinforced joist with the timber grain parallel to the joist axis. In both cases, the reinforcement has been glued to the joist with a phenol-resorcinol adhesive together with self-tapping screws d=5 mm and l=50 mm. Also, a specimen with non-structural glue was tested. Different quantities of glue and number of screws were tested (Table 1).

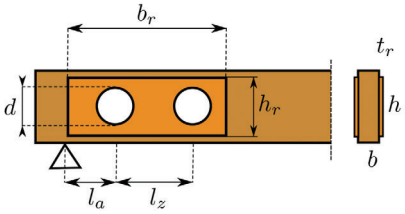

Figure 2 - *Geometry of holes reinforcement*

Table 1*: Mechanical and geometrical properties of the configurations.*

Configuration name	holes (n°)	l_a (m)	l_z (m)	Reinforcement	External lamellae	Specimen (n°)
REF-C30	0	-	-	-	C30	15
UNR-C30-2.7	1	2.7	-	-	C30	10
UNR-C30-0.6-0.6	2	0.6	0.6	-	C30	10
REIN-C30-0.6-0.6-PLY1	2	0.6	0.6	Plywood, PRF 500g/m^2, 8 screws	C30	3
REIN-C30-0.6-0.6-PLY2	2	0.6	0.6	Plywood, PRF 300g/m^2, 8 screws	C30	1
REIN-C30-0.6-0.6-PLY3	2	0.6	0.6	Plywood, Non-struct. glue, 8 screws	C30	1
REIN-C30-0.6-0.6-GL	2	0.6	0.6	Glulam, PRF 300g/m^2, 6 screws	C30	3
DIC-UNR-C30-0.6-0.6	2	0.6	0.6	-	C30	2
DIC-REIN-C30-0.6-0.6	2	0.6	0.6		C30	2
REF-C40	0	-	-	-	C40	20
UNR-C40-2.7	1	2.7	-	-	C40	10
UNR-C40-0.6	1	0.6	-	-	C40	10
UNR-C40-1.7	1	1.7	-	-	C40	10
UNR-C40-0.6-0.6	2	0.6	0.6	-	C40	10
UNR-C40-2.4-0.6	2	2.4	0.6	-	C40	10

2.2 TEST METHODS

The glulam joists were tested according to the four-point bending test procedure outlined in the EN-408 standard [31]. The distance between the base supports was set to l_s=18h=5400 mm, and the distance between a loading points position and the nearest support has been set to a=6h=1800 mm (Figure 1).

The bending strength f_m has been determined with the following equation:

$$f_m = \frac{F_{max} a}{2W} \quad (1)$$

Where F_{max} is the overall maximum load applied by the two jacks, a is the loading points distance from the nearest support and $W=bh^2/6$ is the section modulus.

The global modulus of elasticity in bending $E_{m,g}$ has been calculated from the load-deflection linear regression between F_1 and F_2 and the corresponding deflections w_1 and w_2. The global displacement was measured using LVDT placed under the beams at mid-span, as outlined by the standard. According to EN 408 $F_1=0.1F_{max}$ and $F_2=0.4F_{max}$ or at least $F_2=0.3F_{max}$ with $R2>0.99$, and $w_1=w(F_1)$ and $w_2=w(F_2)$.

The following equation gives the global modulus of elasticity in bending:

https://doi.org/10.52202/069179-0353

$$E_{m,g} = \frac{l^3(F_2 - F_1)}{bh^2(w_2 - w_1)}\left[\left(\frac{3a}{4l}\right) - \left(\frac{a}{l}\right)^3\right] \quad (2)$$

where l is the beam span and $a=6h=l/3$ is the distance from support to the nearest load application point.
The shear strength of the glue line parallel to the direction of the grain of glulam-glulam and glulam-plywood specimens has been tested according to EN-392. The shear test was carried out on specimens with rectangular parallelepiped shapes with two sides of length b=50 mm and the third of t=36 mm or t=48 mm. The offset between each half of the specimen was b_o=5 mm (Figure 3).

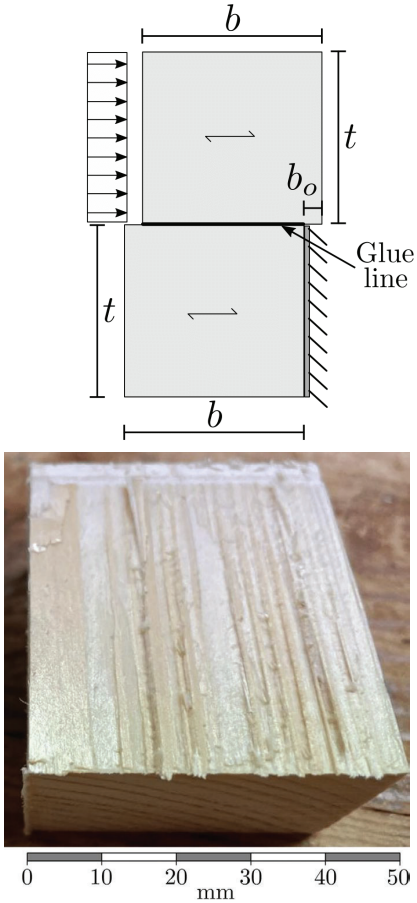

Figure 3 - *Shear tests: (up) dimension and setup; (down) failure surface*

2.3 TEST RESULTS

The overall applied force-midspan deflection results are reported in Figure 4 and Figure 5. The maximum load, the ultimate displacement, the global modulus of elasticity in bending and the bending strength are reported in Table 2. In the reference configurations without holes and configurations with holes in the constant moment area, the joists fail in bending. In contrast, in the joists with one or two holes in the constant shear area, the failure happens due to the longitudinal cracks around the holes (Figure 6).

No appreciable maximum load reduction was observed in configurations with a single hole at midspan (l_a=*2.7 m*). An appreciable decay of the strength of the joist was observed for single hole configurations with l_a=*0.6 m* or l_a=*1.7 m*. The double hole configurations with $l_a=l_z$=*0.6 m* led to the greater reduction in strength of -27% and -33% for C30 and C40 test series, respectively.
The reinforcement of the joists with $l_a=l_z$=*0.6 m* led to a total recovery of the resistance. No significant differences were found in the percentage of strength recovery for varying reinforcement configurations.

Regarding the shear tests, the shear strength and the percentage of timber and glue failures are reported in Table 3. It is worth noting that since the percentage of the timber failure is predominant, the τ_{max} is intended as the shear strength of timber in the direction parallel to the grain.

2.4 PREDICTED LOAD VIA STANDARD FORMULATION

The experimental results have been compared with the predicted load of the formulation prescribed in the DIN-1052. According to the formulation given by this standard, the failure load can be predicted by superposing the effects in terms of traction perpendicular to the grain of the shear and moment component as in the following equation:

$$F_{t,90} = F_{t,V} + F_{t,M} \quad (3)$$

where the shear component $F_{t,V}$ is calculated by integrating the shear tension according to the Euler-Bernoulli theory over the section area delimited by the crack. This area is conventionally defined by the intersection of a 45° line from the hole centre with the hole circumference itself:

$$F_{t,V} = \frac{Vh_d}{4h}\left[3 - \left(\frac{h_d}{h}\right)^2\right] \quad (4)$$

where V is the shear force in the beam, h_d is equal to $d \cdot cos(\pi/4)$ for circular openings, d is the diameter of the hole, h the height of the section of the beam.
The moment component $F_{t,M}$ is calculated by an empirical equation by Kolb and Epple [32]:

$$F_{t,M} = 0.008\frac{M}{h_r} \quad (5)$$

where M is the bending moment in the beam and h_r depends on the remaining height above (h_{ro}) or underneath (h_{ru}) the hole crack and can be assumed equal to $h_r=min(h_{ro}+0.15h_d;\ h_{ru}+0.15h_d)$.

https://doi.org/10.52202/069179-0353

Table 2: *Mean experimental results and coefficients of variation of four-point bending tests. B = failure due to bending, H = failure due to longitudinal cracking around the hole.*

Configuration name	F_{max} (kN)	CoV (%)	F_{max} /$F_{max,REF}$	Failure mode	u_u (mm)	CoV (%)	$E_{m,g}$ (N/mm^2)	CoV (%)	f_m (N/mm^2)	CoV (%)
REF-C30	20.3	12.0	-	B	59.5	14.3	11.0	3.3	33.9	12.0
UNR-C30-2.7	21.4	8.3	1.05	B	61.9	8.3	11.2	5.6	35.6	8.3
UNR-C30-0.6-0.6	14.9	5.8	0.73	H	48.8	10.6	10.5	3.5	24.8	5.8
REIN-C30-0.6-0.6-PLY1	21.9	8.6	1.08	B	64.9	17.3	11.9	7.6	36.5	8.6
REIN-C30-0.6-0.6-PLY2	23.0	0.0	1.13	B	70.4	0.0	11.3	0.0	38.4	0.0
REIN-C30-0.6-0.6-PLY3	22.6	0.0	1.11	B	63.6	0.0	12.2	0.0	37.6	0.0
REIN-C30-0.6-0.6-GL	22.7	5.7	1.12	B	66.3	11.5	12.0	5.5	37.8	5.7
DIC-UNR-C30-0.6-0.6	11.2	8.4	-	H	42.5	15.8	10.2	3.1	18.7	8.4
DIC-REIN-C30-0.6-0.6	12.7	2.4	-	H	47.1	1.1	10.7	0.7	21.2	2.4
REF-C40	31.9	12.2	-	B	58.9	16.3	13.4	3.3	39.9	12.2
UNR-C40-2.7	29.0	10.6	0.91	B	63.6	11.3	11.5	4.7	36.2	10.6
UNR-C40-0.6	26.0	14.4	0.81	H	51.9	17.1	12.3	3.5	32.5	14.4
UNR-C40-1.7	26.0	11.3	0.81	H	55.0	14.4	11.7	3.0	32.5	11.3
UNR-C40-0.6-0.6	21.5	11.5	0.67	H	43.9	13.2	11.7	3.1	26.8	11.5
UNR-C40-2.4-0.6	26.9	10.2	0.84	H	59.9	12.7	11.2	7.3	33.7	10.2

Table 3*: Mean experimental results and coefficients of variation of glue shear tests.*

Configuration name	Specimens (n)	Timber failure (%)	Glue Failure (%)	tau max (MPa)	CoV (%)
PRF Plywood	14	97	3	5.8	23.6
PRF Glulam	10	74	26	7.8	12.3

The load of Eq.3 is then compared to the tensile strength of the area subjected to stresses perpendicular to the grain. It is worth noting that according to this model when the crack is located nearest to the mid-height of the section of the beam, the shear contribution defined in Eq.4 increases while the bending contribution defined in Eq.5 decreases. The results in terms of predicted load and percentage deviations from the experimental load are shown in Table 4. The formulation provides accurate predictions in almost all cases that experimentally exhibit failure due to crack propagation around the holes.

3 FINITE ELEMENT MODELLING

A three-dimensional finite-element model capable of reproducing the joist failure mode due to tensile crack formation was implemented in ABAQUS. The model assembly, analysis and post-processing were performed through a Python script to automatise the process and allow for extended validation and parametric analyses.

3.1 MODEL DESCRIPTION

Due to the symmetry of the joist and holes (see Table 1) in the vertical-longitudinal *yz* plane, it was possible to reproduce only half of the actual geometry. On the symmetry plane, the displacement in the out-of-plane direction was restrained $u_x=0$. The hinge support restraint has been reproduced by imposing $u_y=u_z=0$ on the contact line nodes, whilst the roller restraint has been reproduced by imposing $u_z=0$ on the contact line nodes (Figure 7).
An imposed linearly increasing displacement was applied to the nodes of the contact areas between the beam and the distribution plate under the hydraulic jacks ($u_{imp}=100$ *mm*).
The joist has been discretized through C3D8R general-purpose linear brick element, with reduced integration (ABAQUS/Standard library). The mesh dimensions are approximate $m_s \approx b/4$.

https://doi.org/10.52202/069179-0353

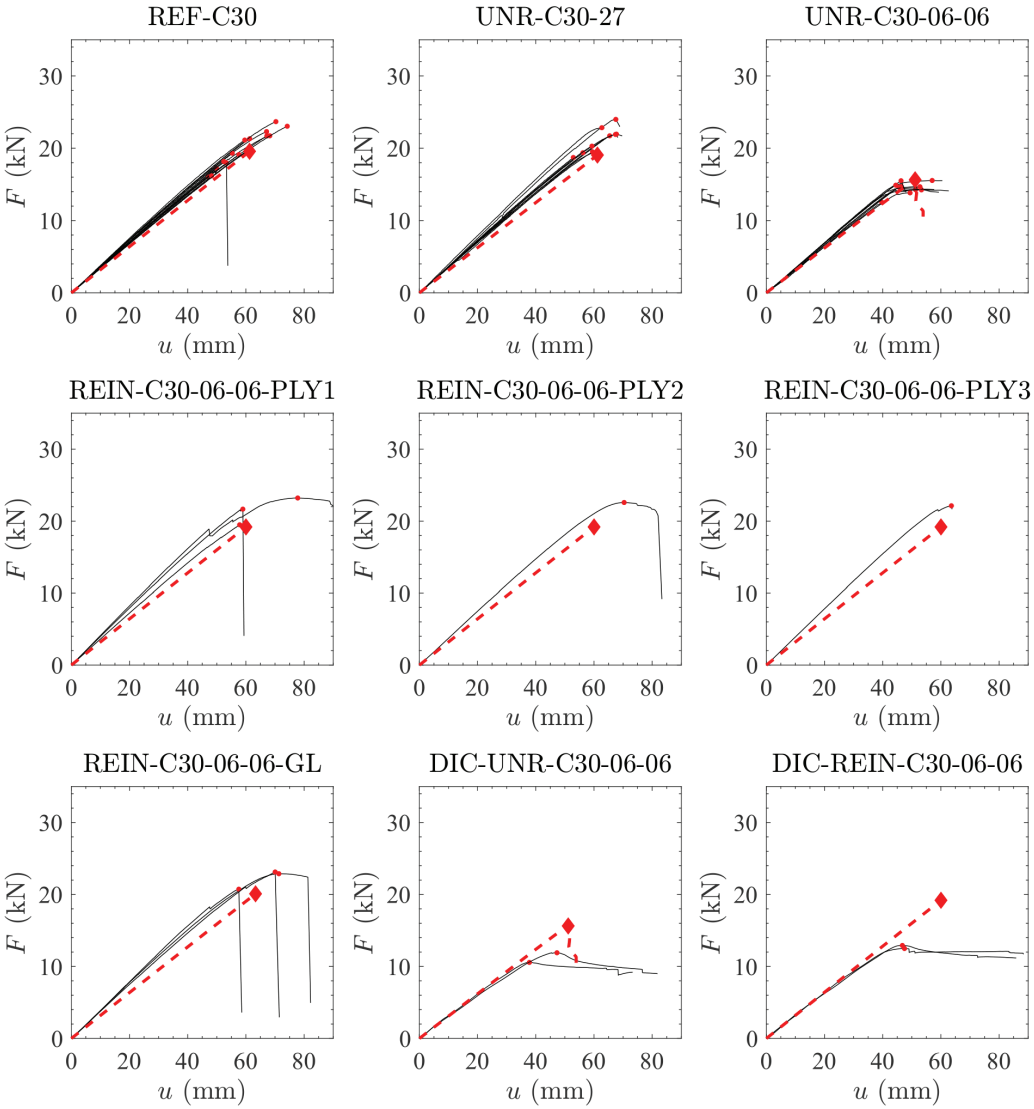

Figure 4: *Force-displacement curves for C30 test series (black line: experimental, red line: finite element model).*

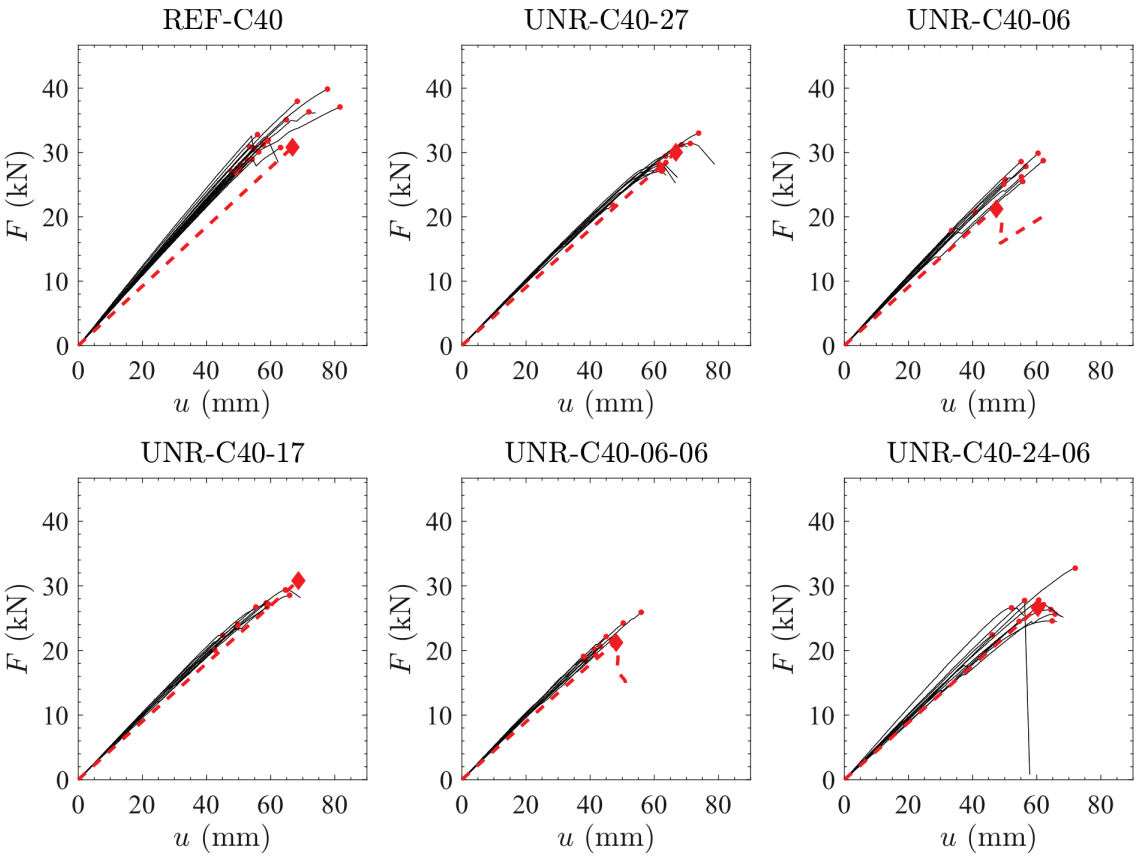

Figure 5: *Force-displacement curves for C40 test series (black line: experimental, red line: finite element model).*

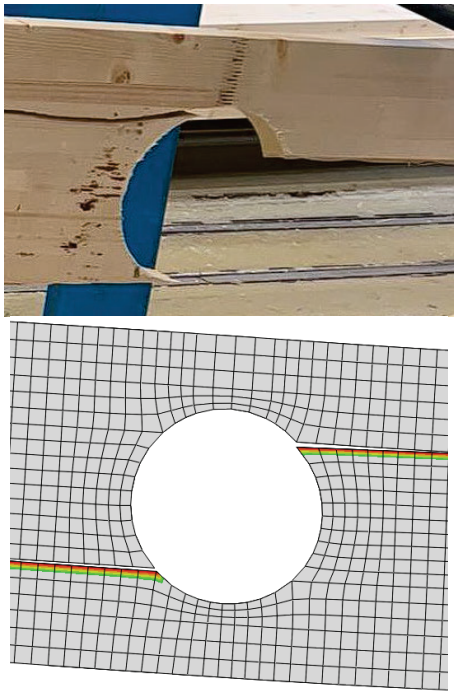

Figure 6: *Hole failure mode: (up) Experimental (down) Finite element model.*

A linear elastic constitutive law has been assigned to outer and inner lamellae domain portions. The material has been modelled as orthotropic and the elasticity moduli and the shear moduli were related to the elastic module in the direction parallel to the grain according to EN-338 [33]. The elastic moduli in the direction perpendicular to the grain have been assumed as $E_x=E_y=E_z/30$, and the shear modules have been assumed as $G_{zy}=G_{zx}=E_z/16$ and the rolling shear moduli has been assumed as $G_{xy}=G_{zy}/10$. Similarly, the plywood reinforcement mechanical properties have been chosen according to EN 13986 and EN 636 and are reported in Table 5.

Cohesive contacts are assigned to surfaces explicitly introduced into the model to reproduce the crack formation and propagation around the hole. No stress interaction was considered for the cohesive layer; the damage is initiated where and when the stresses in the main local direction reach their relative strength values. Conventionally, the crack around the hole is assumed to be at an angle of 45° to the longitudinal axis of the beam. In the finite element models herein developed, the position of the cohesive contacts has been assumed coincident with the point of attainment of the maximum tensile stress perpendicular to the grain on the hole circumference. This position has been determined using preliminary elastic analyses conducted on a single-hole beam} for varying hole positions and both the case of

https://doi.org/10.52202/069179-0353

four-point bending and uniformly distributed load (Figure 8).

***Table 4**: Finite element model results and experimental scatters (*the experimental failure load is due to bending while the DIN predicted failure load is due to hole failure).*

Configuration name	F_{max} (kN)	$S_{FEM-EXP}$ (%)	$E_{m,g,FEM}$ (N/mm^2)	$S_{FEM-EXP}$ (%)	$F_{max,DIN}$ (kN)	$S_{DIN-EXP}$ (%)
REF-C30	19.6	-3.7	11.0	0.2	-	-
UNR-C30-2.7	19.1	-10.9	10.8	-3.8	31.8	48.8
UNR-C30-0.6-0.6	15.6	5.0	10.7	2.0	13.9	-6.6
REIN-C30-0.6-0.6-PLY1	19.2	-12.3	11.1	-7.3		
REIN-C30-0.6-0.6-PLY2	19.2	-16.6	11.1	-2.3		
REIN-C30-0.6-0.6-PLY3	19.2	-14.9	11.1	-8.9		
REIN-C30-0.6-0.6-GL	20.1	-11.4	11.0	-8.2		
DIC-UNR-C30-0.6-0.6	15.6	39.1	10.7	4.5	13.9	23.7
DIC-REIN-C30-0.6-0.6	19.2	51.0	11.1	3.0		
REF-C40	30.8	-3.5	11.9	-10.7	-	-
UNR-C40-2.7	30.0	3.5	11.7	1.5	42.4	46.2
UNR-C40-0.6	21.2	-18.4	11.8	-4.3	21.7	-16.6
UNR-C40-1.7	30.8	18.3	11.7	-0.3	16.5	-36.6
UNR-C40-0.6-0.6	21.2	-1.2	11.6	-1.1	18.5	-13.8
UNR-C40-2.4-0.6	26.6	-1.2	11.5	2.6	42.4	57.3

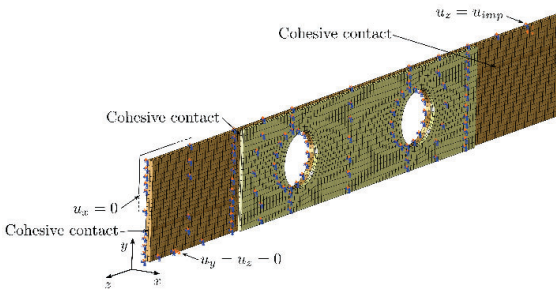

***Figure 7**: Finite element model*

In the case of uniformly distributed load, the maximum stress around the hole is reached between 30° and 40° to the longitudinal axis of the beam with a descending trend if the hole moves towards the mid-span (increasing l_a). Beams with a hole close to the mid-span exhibited lower stresses than those with hole close to the end support. In the four-point bending configuration, tension perpendicular to the grain increases in the part of the beam subjected to linearly increasing bending moment, while a stress drop and a sudden change of the maximum stress location is observed immediately after the loading point location which is at l_a=*6h=1800 mm*. Due to the local effect of the loading point, when the hole is under the external load, the maximum stress is reached near the bottom part of the hole.

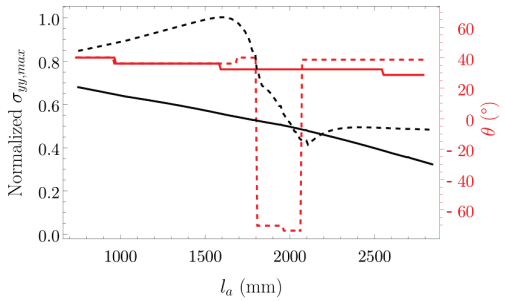

***Figure 8:** Normalized maximum stress and attainment position on the hole circumference for varying hole-support distance l_a (**Figure 1**) (Continuous lines: uniformly distributed load; Dashed lines: four-point bending).*

The interaction between the beam lateral surface and the reinforcement has also been modelled with cohesive contacts to make the model able to predict the failure on the reinforcement-joists contact surface. The screws used to restrain the reinforcement to the beam during the glue curing are neglected in the model. This assumption is made since the stiffness of screws perpendicular to the sliding plane is much lower than the stiffness of the glued connection and therefore, when the reinforced system fails, the contribution of the screws in terms of forces is negligible [34, 35].

The cohesive contacts are specialized constitutive laws used to simulate crack initiation and propagation [21]. Despite timber exhibiting exponential softening behaviour in experimental fracture tests, a bilinear curve is commonly used for this traction-separation curve [36].

The cohesive contacts behaviour is governed by a damage initiation criterion and a traction-separation curve, which relates element traction (stress) to *mode I* (opening) and *mode II* (shearing) displacement.
The bilinear traction-separation relationship consists of an initial elastic region showing the interfacial strength; and a subsequent softening region where zero stress is reached (see Figure 9). *D* is the damage parameter, which changes from *D=0* in the undamaged state to *D=1* in the fully damaged state:

$$D = \frac{\delta_e(\delta - \delta_c)}{\delta(\delta_e - \delta_c)} \quad (6)$$

δ_c indicates the separation corresponding to damage initiation, and δ_e is the final separation corresponding to the full fracture of the element. The total area under the curve is the fracture energy of the material. The stress-strain relationship is assumed for material outside the fracture process zone, and the stress versus separation curve is used for the material in the fracture process zone. However, the traction-separation laws become active only after a damage initiation criterion is met, e.g., when the stress exceeds the material's strength. When it comes to damage evolution, Wu's mixed mode fracture criterion was used [37, 38]:

$$\left(\frac{G_I}{G_{IC}}\right)^m + \left(\frac{G_{II}}{G_{IIC}}\right)^n = 1 \quad (6)$$

G_I and G_{II} indicate the fracture energies for mode I and II, respectively, and G_{IC}, G_{IIC} instead their critical energy release rate values, m and n denote the power of the equation.
The damage initiation parameters σ_n and τ_l have been chosen equal to the inner lamellae tensile strength in the direction perpendicular to the grain and inner lamellae shear strength in the direction parallel to the grain, as explained in the following paragraphs. The shear strength is assumed from experimental tests. In contrast, the tensile strength perpendicular to the grain derives from the model calibration using the experimental test results of the beams in terms of ultimate load. The propagation parameters of the cohesive contact have been chosen according to the results of [21] and are reported in Table 6.
According to [39], the critical fracture energy G_{IC} for mode I varies between 150-600J/m^2 for softwood species. In contrast, the critical fracture energy for mode II can be assumed as $G_{IIC}=3G_{IC}$.

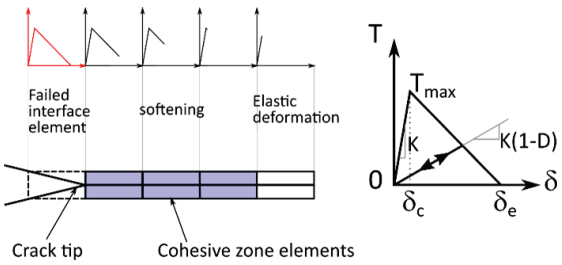

***Figure 9**: Cohesive elements and traction separation curve.*

3.2 MODEL CALIBRATION AND VALIDATION

Firstly, the elastic properties (i.e. the MoE perpendicular to grain, and the shear modulus) of the external and internal lamellae were calibrated according to the reference test series without holes. A sensitivity analysis was conducted on the numerical model to investigate which combination of parameters would minimise the difference with the experimental results. The investigated parameters were the elastic moduli perpendicular to grain and the shear modulus of both the external and internal lamellae. The bounds of the sampling domain were set to $E_{z,ol}$=*13 GPa ±25%,* $G_{zy,ol}=G_{zx,ol}$=*0.75 GPa ±25%,* $E_{z,il}$=*9 GPa ±25%,* $G_{zy,il}=G_{zx,il}$=*0.56 GPa ±25%.* The domain was sampled adopting Saltelli's sampling scheme [40, 41]. The error between the experimental and numerical results was assessed by the squared difference of the ratio of the applied force to the displacement at mid-span (SS).
A graphical representation of the results is shown in Figure 10. Here each point is a triplet of values $E_{z,il}$, $E_{z,ol}$ and the squared differences in terms of stiffness between the experimental and finite element model results) with the two MoE shown on the two horizontal axis. The figure clearly shows that a combination of values that minimises the error exists. By imposing a low threshold value for the error and fitting with linear regression, a relation between $E_{z,il}$ and $E_{z,ol}$ were found. The analysis confirmed also that the shear moduli $G_{zy,il}$ did not have any effect on the results.

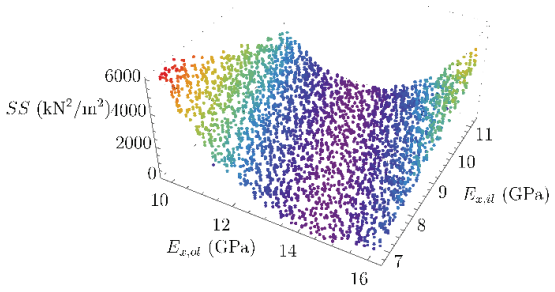

***Figure 10**: Squared differences in terms of stiffness between the experimental and finite element model results for various combinations of $E_{z,ol}$, $E_{z,il}$ and $G_{zy,il}$.*

Experimental tests carried out on the outer lamellae provided a mean value for $E_{z,ol}$ equal to 14.5 and 12.5 for the C40 and C30 timber. Therefore, assuming the above values for the MoE of the outer lamellae, the estimated value of the MoE of the inner lamellae is $E_{z,il}$≈10.5 GPa. The resume of all mechanical parameters is shown in Table 5.

In the second stage, the parameters governing the cohesive contact of the beam and the reinforcement were studied. Since the results of the shear test of glued specimens had demonstrated that the failure happens mainly on the timber side, the shear damage initiation parameter τ_l was assumed equal to the experimentally determined value, which corresponds to the actual shear strength of glulam (Table 3 and Table 6).

https://doi.org/10.52202/069179-0353

***Table 5**: Mechanical properties.*

Material name	E_z (Gpa)	$E_x = E_y$ (Gpa)	$G_{zy} = G_{zx}$ (Gpa)	G_{xy} (Gpa)	ν
C40	14.5	0.48	0.91	0.091	0.4
C30	12.5	0.42	0.78	0.078	0.4
Inner lamellae	10.5	0.35	0.66	0.066	0.4
Plywood	8	6	0.35	0.05	0

The tensile strength perpendicular to the grain σ_n and the fracture energy G_{IC} was estimated by minimizing the error between the numerical and experimental result of the unreinforced beams in terms of ultimate load.
The parameter G_{IIC} was derived from the previously mentioned relation according to [39].

A comparison between the results of the calibrated models and the test results is shown in Figure 4 and Figure 5 and Table 4.

***Table 6:** Mechanical properties of the choesive contacts.*

	σ_n (MPa)	τ_I (MPa)	G_{IC} (J/m^2)	G_{IIC} (J/m^2)	m	n
Inner lamellae	1.2	7.9	400	1200	0.5	0.5
Reinforcement Joist	5.4	5.8	400	1200	0.5	0.5

Overall a good agreement between experiments and numerical simulations is achieved. The elastic analyses confirmed that the crack starts at about 28-40° with respect to the longitudinal axis of the beam (Figure 8), which is a well-known result in literature [1, 39] and also confirmed by the experimental outcomes Figure 6.
In some cases (e.g. hole at mid-span, reinforced holes) the cohesive layer failed when the stress perpendicular to the grain on the outermost fibre had already passed values that would have led to a bending failure of the beam. For this reason, an additional failure criterion based on the tensile stresses reached in the outermost elements was introduced. The ultimate tensile stress was assumed to be equal to the one found by the tests on the reference beam, and namely f_m=33.9 MPa and f_m=39.9 for C30 and C40 test series respectively.

3.3 PARAMETRIC ANALYSES

In this section, the results of some parametric studies performed to identify the parameters that have the greatest impact on the ultimate load of the joists are reported.
It is assumed in the finite element models of all studied cases that the external lamellae are strong enough to avoid the bending failure of the joist. In this way, the finite element model can only account for the combined shear-tension perpendicular to the grain failure, so the hole is always the weak point from which the cracks that lead to the failure of the joist propagate.\\
The following plots show the failure load associated with the hole crack propagation determined through the parametric finite element model (contour of Figure 11, Figure 12 and). On the same plots, the analytically determined flexural limit loads of the joist mid-span section (grey surface) and of the hole section (magenta surface) are reported. The flexural limit loads have been determined as the loads which cause the tensile failure of the outermost lamella accounting for the heterogeneous section and the hole in the section modulus calculation (W_{ef} and $W_{ef,hole}$ respectively). The associated maximum forces have been determined from Navier's equation. For the mid-span failure load:

$$f_m = \frac{M_{max}\left(\frac{l}{2}\right)}{W_{ef}\left(\frac{E_{ol}}{E_{il}}, h_{ol}, h_{il}\right)} \tag{8}$$

and for the hole-section failure load:

$$f_m = \frac{M_{max}(l_a + l_s)}{W_{ef,hole}\left(d, \frac{E_{ol}}{E_{il}}, h_{ol}, h_{il}\right)} \tag{9}$$

By substituting in Eqs. 8 and 9 the expression of bending moment M_{max} as function of F_{max} for uniformly distributed load or four-bending configuration and solving for F_{max} the corresponding expressions for the analytically determined bending capacity F_a were found:

$$F_{max} = \begin{cases} \frac{2f_m W_{ef}}{l} \; mid\ span, unif.dist. \\ \frac{2f_m W_{ef,hole} l}{(l_a+l_z)(l-l_z-l_z)} \; hole, unif.dist \\ \frac{2f_m W_{ef}}{a} \; mid\ span, 4\,p.b. \\ \frac{2f_m W_{ef,hole}}{l_a+l_z} \; hole\ and\ l_a + l_z \le a, 4\,p.b. \\ \frac{2f_m W_{ef,hole}}{a} \; hole\ and\ l_a + l_z > a, 4\,p.b. \end{cases}$$

The first parametric study identifies the influence of hole diameter and hole position for a four-point bending configuration. As can be seen from Figure 11 (up) which shows the results for joists similar to that of configuration UNR-C30-0.6-0.6, moving the two holes closer to the load application point causes a slight increase in strength of the hole-failure mechanism. As shown in Figure 8, when the hole is about at 1_d from the load application point l_a=*1.5 m*, the external load-induced compression perpendicular to the grain causes a significant reduction of the tensile stresses (Figure 8).

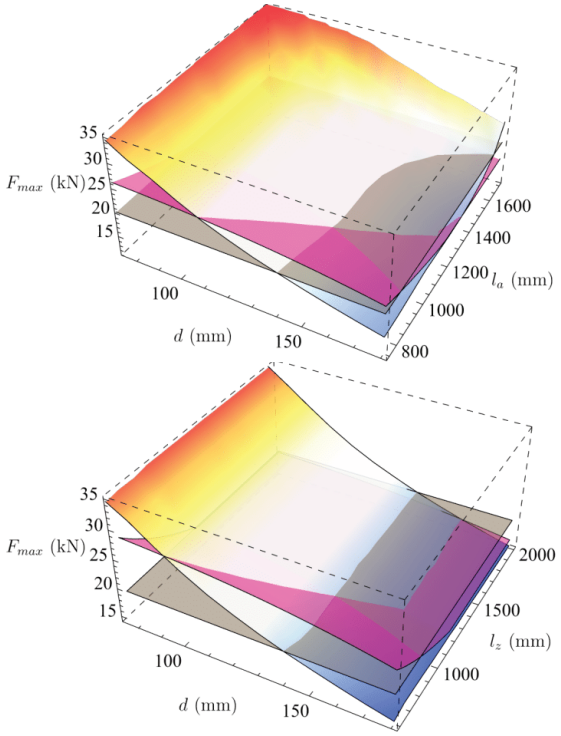

***Figure 11**: Failure load for varying hole diameter and hole position in four-point bending configuration: (up) varying the position of both holes simultaneously (l_a), (down) varying second hole position (l_z) (Contour: FEM hole crack failure load, gray: failure load of mid-span section without hole, magenta: failure load of hole-section).*

Keeping fixed the position of the hole nearest to the support l_a=*0.6 m*) and moving the position of the second hole does not affect the capacity associated with the hole failure because the limit load is related to the failure of the first hole (Figure 11 (down)). In both cases, the hole diameter has a strong influence on the strength reduction.

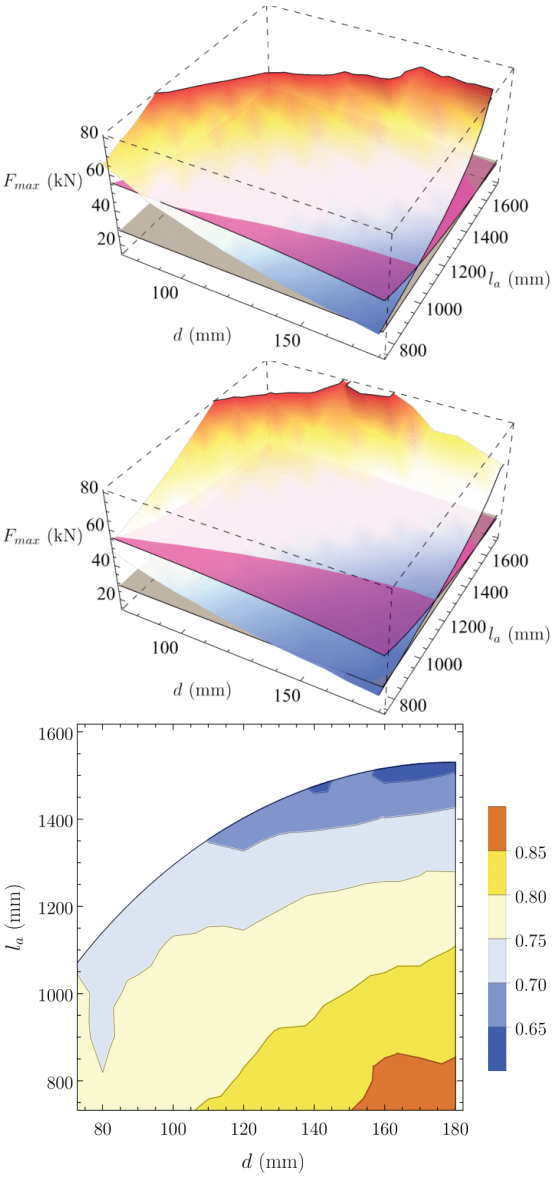

***Figure 12**: Failure load for varying hole diameter and hole position in the uniformly distributed configuration: (up) load at the upper side, (mid) load at the lower side, (down) ratio between the failure load of the lower side and upper side. (Contour: FEM hole crack failure load, grey: failure load of mid-span section without hole, magenta: failure of hole-section*

The second set of parametric studies deals with the case of uniformly distributed load. In both the cases of load applied at the lower side of the beam and load applied at the upper side of the beam, the hole position has proven to be a more significant parameter than in four-point bending configuration in determining the ultimate load for hole area-cracking failure mode (Figure 12). This behaviour is justified by the different arrangements of the internal forces. In the four-point bending configuration, the hole position was varied along the part of the beam in constant shear and linearly increasing bending moment, whilst in uniformly distributed load configuration the beam is subjected to linearly decreasing shear towards the mid-span and parabolic bending moment. As a

https://doi.org/10.52202/069179-0353

consequence when increasing l_a in a four-point bending configuration the tensile stresses perpendicular to the grain due to the combined shear and bending effect increases and reduce only when the local effect of the external load is significant, whilst in uniformly distributed load configuration an almost linear reduction of tensile stresses perpendicular to the grain for increasing l_a can be observed (Figure 8).

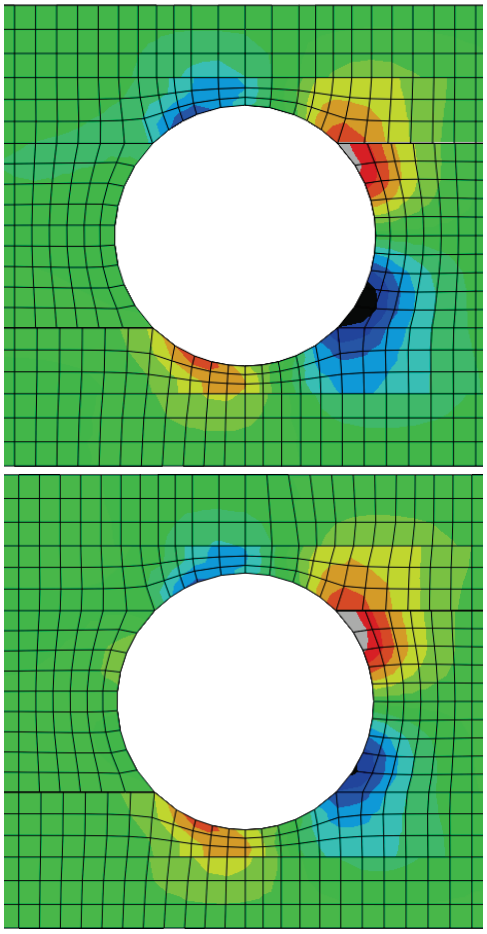

***Figure 13**: Tensile stresses perpendicular to the grain: (up) upper side load, (down) lower side load.*

Applying the load at the lower side causes a reduction in the ultimate load comprised between 40% and 15%. For fixed hole position the reduction is higher for lower diameters. The closer the hole is near the midspan, the higher the reduction. It was observed that applying the same load at the lower side causes an increase in the tensile stresses perpendicular to the grain around the hole (Figure 13).

In the last parametric study, the height of the beam h=300 mm and the relative position of the hole $l_a/l = 0.1$ were maintained constant while varying the length of the beam l and the hole diameter d. This study revealed how for shorter-span beams, the influence of the hole diameter is higher with respect to longer-span beams (Figure 14).

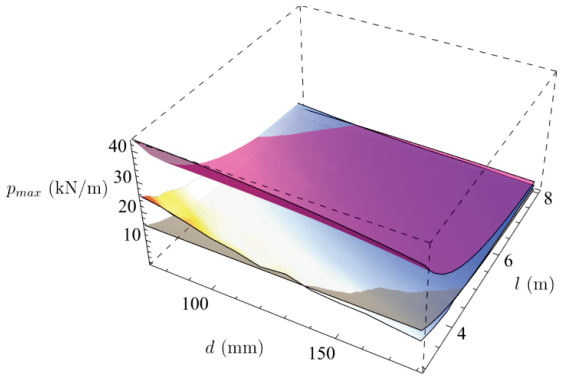

***Figure 14**: Failure load for varying hole diameter and beam length. (Contour: FEM hole crack failure load, grey: failure load of mid-span section without hole, magenta: failure load of hole-section).*

4 CONCLUSIONS

An extended experimental investigation has been conducted on composite glulam joists. The tests highlighted strength reductions up to 33% when in a four-point bending configuration the hole is located in the constant shear zone. No significant differences were found between plywood and glulam reinforcements or between PRF and non-structural glue types. In all cited cases a complete restoration of the joist bending strength was observed.

The developed finite element model provided accurate results in terms of strength and stiffness. The results of the parametric study can be itemized as follow:

- the hole position is a more relevant parameter in beams loaded by a uniformly distributed load than in beams under four-point bending;
- in four-point bending configuration the applied load prevents crack formation; so when the hole is under the load application point the failure load increase;
- applying the load at the lower side causes a reduction in the ultimate load comprised between 40% and 15% with respect to applying the load at the upper side;
- the strength reduction caused by the hole is more pronounced for shorter span beams

Although a satisfying correspondence was found between the formulation provided by the DIN-1052 and the experimental results, the authors proposed a mechanics-based probabilistic formulation for the determination of the strength reduction of beams with holes. Both the case of uniformly distributed load applied at the upper side and lower side have been considered. The proposed formulas are elementary and therefore could be implemented in codes or easily used by practitioners as a possible improvement of the current experimentally derived formulation.

https://doi.org/10.52202/069179-0353

ACKNOWLEDGEMENT

Enter acknowledgements directly before the references. Use the format of primary section headers, but do not number the acknowledgement and references sections.

REFERENCES

1. Aicher, S., L. Höfflin, and H.W. Reinhardt, *Runde durchbrüche in biegeträgern aus brettschichtholz–teil 2: tragfähigkeit und bemessung.* Bautechnik, 2007. **84**(12): p. 867-880.
2. Ardalany, M., B.L. Deam, and M. Fragiacomo, *Numerical investigation of the load carrying capacity of Laminated Veneer Lumber (LVL) joists with holes*, in *11th World Conference on Timber Engineering 2010, WCTE 2010*. 2010. p. 690-699 ,.
3. Danielsson, H., The Strength of Glulam Beams with Holes: A Survey of Tests and Calculation Methods, 2007: p. 1-91 ,.
4. Foliente, G.C. and T.E. McLain, *Strength of end-notched wood beams: A critical fillet hoop stress approach.* Wood Fiber Sci., 1992. **24**(2): p. 168-180 ,.
5. Lee, Y.C., A Study of the Elastic Stresses Around Holes in A Wide-flange Beam with A Concentrated Load, 1969.
6. Smith, C.B., *Mimeo 1510: Effect ofElliptic or Circular Holes on the Stress Distribution in Plates of Wood or Plywood Considered as Orthotropic Materials.* Effect of Elliptic or Circular Holes on the Stress Distribution in Plates of Wood or Plywood Considered As Orthotropic Materials, 1944.
7. Danielsson, H. and P.J. Gustafsson, *Strength of glulam beams with holes-Tests of quadratic holes and literature test result compilation, International Council for Research and Innovation in Building and Construction, Working Commission W18-Timber Structures.* Cib-W18, 2008.
8. Danielsson, H. and P.J. Gustafsson, *A probabilistic fracture mechanics method and strength analysis of glulam beams with holes.* European Journal of Wood and Wood Products, 2011. **69**(3): p. 407-419.
9. Schmidt, J. and M. Kaliske, *Simulation of cracks in wood using a coupled material model for interface elements.* Holzforschung, 2007. **61**(4): p. 382-389.
10. Carling, O., Swedish Glulam Handbook, 2001.
11. Zhu, E.C., et al., *Effect of openings on oriented strand board webbed wood I-joists.* Journal of Structural Engineering, 2007. **133**(1): p. 145-149.
12. Morrissey, G.C., D.W. Dinehart, and W.G. Dunn, *Wood I-joists with excessive web openings: An experimental and analytical investigation.* Journal of Structural Engineering, 2009. **135**(6): p. 655-665.
13. Shahnewaz, M., et al., *Reinforced Wood I-Joists with Web Openings.* Journal of Structural Engineering (United States), 2017. **143**(6).
14. Guan, Z.W. and E.C. Zhu, *Finite element modelling of anisotropic elasto-plastic timber composite beams with openings.* Engineering Structures, 2009. **31**(2): p. 394-403.
15. Zhu, E.C., et al., *Finite element modelling of OSB webbed timber I-beams with interactions between openings.* Advances in Engineering Software, 2005. **36**(11-12): p. 797-805.
16. Danzer, M., P. Dietsch, and S. Winter. *Reinforcement of round holes in glulam beams arranged eccentrically or in groups*. in *World Conf. on Timber Eng*. 2016.
17. Aicher, S. and L. Höfflin, *Glulam beams with holes reinforced by steel bars.* Intl. Council for Research and Innovation in Building and Construction, Working Commission 18-Timber Structures, 2009.
18. Karimi-Nobandegani, A. and H. Valipour, *Effect of web openings on timber composite beams: Testing and analytical modelling.* Engineering Structures, 2022. **256**(January): p. 114064.
19. Karimi-Nobandegani, A. and H. Valipour, *Timber beams with openings: Laboratory testing and nonlocal finite element modelling.* Engineering Structures, 2021. **245**.
20. Gilbert, B.P., et al., *Veneer-based timber circular hollow section beams: behaviour, modelling and design.* Construction and Building Materials, 2020. **258**: p. 120380.
21. Ardalany, M., M. Fragiacomo, and P. Moss, *Modeling of Laminated Veneer Lumber Beams with Holes Using Cohesive Elements.* Journal of Structural Engineering (United States), 2016. **142**(1).
22. Aicher, S., Fracture Mechanics Models for Strength Analysis of Timber Beams with A Hole or A Notch: A Report of RILEM TC-133, 1993.
23. Aicher, S., J. Schmidt, and S. Brunold, *Design of timber beams with holes by means of fracture mechanics.* Proc. CIB Working Commission 18: Timber Structures Meeting 28, 1995.
24. Gustafsson, P.J., *Mean stress approach and initial crack approach.* Fracture Mechanics Models for Analysis of Timber Beams with A Hole or A Notch-a Report of RILEM TC-133. Report TVSM-7134, 2002.
25. Aicher, S. and L. Hofflin, Fracture Behavior and Design of Glulam Beams with Round Holes, 2008.
26. Ardalany, M., *Analysis and Design of Laminated Veneer Lumber Beams with Holes.* Thesis, 2012(September): p. 315.
27. Guan, Z.W. and E.C. Zhu, *Nonlinear finite element modeling of crack behavior in oriented strand board webbed wood I-beams with openings.* Journal of Structural Engineering, 2004. **130**(10): p. 1562-1569.
28. Serrano, E. and P.J. Gustafsson, *Fracture mechanics in timber engineering - Strength*

https://doi.org/10.52202/069179-0353

analyses of components and joints. Materials and Structures/Materiaux et Constructions, 2007. **40**(1): p. 87--96.
29. Sandhaas, C., J. Van de Kuilen, and H.J. Blass. *A 3D constitutive wood model using the concepts of continuum damage mechanics*. in *CDROM Proceedings of the 6th European Congress on Computational Methods in Applied Sciences and Engineering (ECCOMAS 2012), Vienna University of Technology, Austria, iSBN*. 2012.
30. Gharib, M., et al., *Three-dimensional constitutive modelling of arbitrarily orientated timber based on continuum damage mechanics.* Finite Elements in Analysis and Design, 2017. **135**: p. 79-90.
31. *BS EN 408, Timber structures - Structural timber and glued laminated timber - Determination of some physical and mechanical properties.* BSI Standards Limited, 2012.
32. Kolb, H., *Verstärkung von durchbrochenen Brettschichtbindern*. 1985: Forschungs-und Materialprüfungsanst. Baden-Württemberg.
33. *BS EN 338, Structural timber—Strength classes.* BSI Standards Limited., 2009.
34. Yuri De, S. and F. Massimo, *Timber-to-timber and steel-to-timber screw connections: Derivation of the slip modulus via beam on elastic foundation model.* Engineering Structures, 2021. **244**: p. 112798 , publisher = Elsevier Ltd.
35. Tannert, T., A. Gerber, and T. Vallee, *Hybrid adhesively bonded timber-concrete-composite floors.* International Journal of Adhesion and Adhesives, 2020. **97**.
36. Harper, P.W. and S.R. Hallett, *Cohesive zone length in numerical simulations of composite delamination.* Engineering Fracture Mechanics, 2008. **75**(16): p. 4774-4792.
37. Jernkvist, L.O., *Fracture of wood under mixed model loading I. Derivation of fracture criteria.* Engineering Fracture Mechanics, 2001. **68**(5): p. 549-563.
38. Jernkvist, L.O., *Fracture of wood under mixed model loading II. Experimental investigation of Picea abies.* Engineering Fracture Mechanics, 2001. **68**(5): p. 565-576.
39. Blaß, H.J. and C. Sandhaas, *Timber engineering-principles for design*. 2017: KIT Scientific Publishing.
40. Francesca, C., S. Andrea, and C. Jessica, *From screening to quantitative sensitivity analysis. A unified approach.* Computer Physics Communications, 2011. **182**(4): p. 978-988.
41. Sobol, I.M., *Global sensitivity indices for nonlinear mathematical models and their Monte Carlo estimates.* Mathematics and Computers in Simulation, 2001. **55**(1): p. 271-280.